ADVANCED MATERIALS TECHNOLOGIES
www.advmattechnol.de

Highly Efficient and Water-Stable Lead Halide Perovskite Quantum Dots Using Superhydrophobic Aerogel Inorganic Matrix for White Light-Emitting Diodes

Zongtao Li, Cunjiang Song, Jiasheng Li, Guanwei Liang, Longshi Rao, Shudong Yu, Xinrui Ding, Yong Tang, Binhai Yu, Jianzhen Ou, Uli Lemmer, and Guillaume Gomard*

At present, most of lead halide perovskite quantum dots (PQDs) embedded in an enclosed organic polymer or glass matrix can achieve high water stability, yet this limits their subsequent integration with light-emitting diodes (LEDs) and other functional materials. Herein, a postadsorption process using superhydrophobic aerogel inorganic matrix (S-AIM) with open structures is presented to enhance water stability of PQDs and compose new functions to them such as magnetism. The $CsPbBr_3$ PQDs integrated with the S-AIM (AeroPQDs) exhibit a high relative photoluminescence quantum yield (PLQY, 75.6%) of 90.9% compared to pristine PQDs (PLQY, 83.2%). They preserve their initial PL intensity after 11 days of soaking in water and achieve a high relative PLQY stability (50.5%) after soaking for 3.5 months. The hydrophobic (rough) surface of the matrix, its pores with a well-matched mean diameter that promotes the homogeneous integration of PQDs and hinders the penetration of water as well as the oleophylic functional groups covering the surface of these pores are the three factors responsible for the high water stability. Finally, AeroPQDs are easily integrated with other functional nanomaterials, such as Fe_3O_4 nanoparticles for magnetic manipulation, due to their open structure.

1. Introduction

Lead halide perovskite quantum dots (PQDs) are highly suitable for wide-gamut display applications as they exhibit ultrahigh photoluminescence quantum yields (PLQYs), a narrow emission full-width at half maximum (FWHM), and a tunable emission wavelength.[1–6] Among them, inorganic PQDs achieve higher stabilities than organic–inorganic protected PQDs, and hence have drawn a lot of attention as down-conversion materials for white light-emitting diodes (WLEDs).[7–10] For practical applications, the cost-effectiveness, the optical performance, and the stability of PQDs should be further improved.[4] Particularly, PQDs suffer from low chemical and optical stabilities, resulting in their fast degradation under exposure to moisture, heat, and light irradiance.[11,12] Accordingly, PQDs exhibit much lower stability than conventional rare-earth-based phosphor materials.[13,14] Current research efforts therefore aim at enhancing the stability of PQDs by covering them in inorganic materials, including CdS,[15] zeolite,[16,17] glass,[18,19] CaF_2,[20] Al_2O_3,[21–23] SiO_2,[24–29] and TiO_2.[30] Generally, the protective shells of PQDs are prepared using these inorganic materials by in situ synthesis. While protected PQDs with high chemical, thermal, and irradiation stabilities have been obtained,[28] the water stability of PQDs prepared with these inorganic shells still indicate a lot of room for improvement. For instance, the PL intensity of CaF_2 shell-integrated green PQDs reduces to <50% after a water-resistance test of ≈40 h.[20]

Consequently, and until now, PQDs with high water stability are achieved by embedding them in enclosed organic polymer and glass matrices.[18,19,31–39] The hydrophobic surface and dense polymer chains of the matrix can effectively protect the PQDs from the external environment, considerably enhancing their

Prof. Z. Li, Dr. C. Song, Dr. J. Li, Dr. G. Liang, Dr. L. Rao, Dr. S. Yu, Prof. X. Ding, Prof. Y. Tang, Prof. B. Yu
Engineering Research Center of Green Manufacturing for Energy-Saving and New-Energy Technology
South China University of Technology
Guangdong 510640, China
E-mail: jiasli@foxmail.com

Prof. Z. Li, Dr. J. Li
Foshan Nationstar Optoelectronics Company Ltd.
Foshan 528000, China

The ORCID identification number(s) for the author(s) of this article can be found under https://doi.org/10.1002/admt.201900941.

Prof. J. Ou
School of Engineering
RMIT University Melbourne
Melbourne, Victoria 3001, Australia

Prof. U. Lemmer
Light Technology Institute
Karlsruhe Institute of Technology (KIT)
Engesserstrasse 13, Karlsruhe 76131, Germany

Prof. G. Gomard
Institute of Catalysis Research and Technology
Karlsruhe Institute of Technology (KIT)
Eggenstein-Leopoldshafen, Karlsruhe 76344, Germany

DOI: 10.1002/admt.201900941

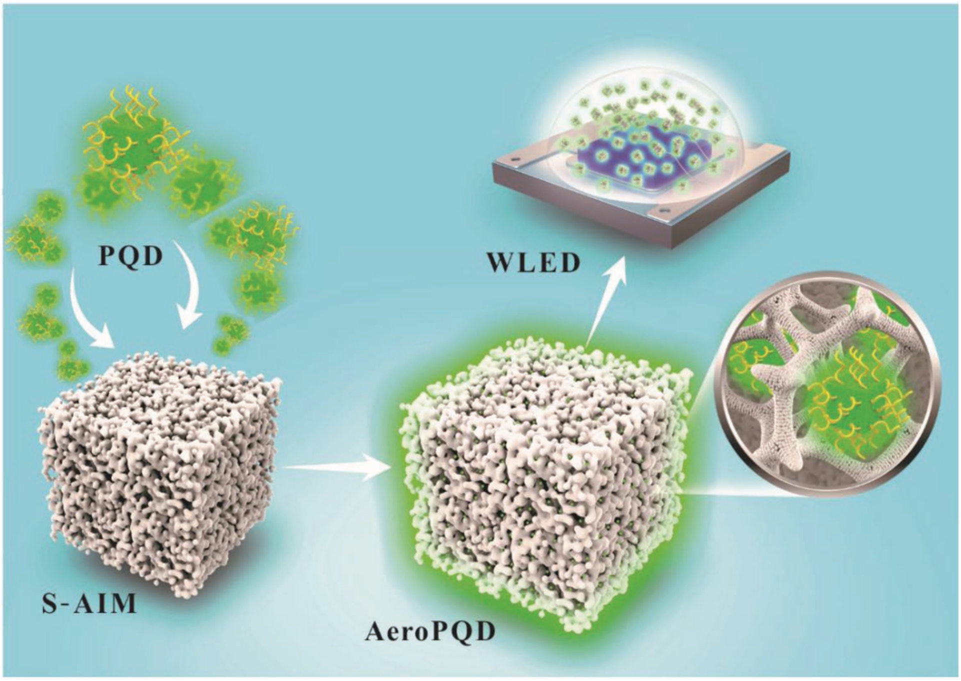

Figure 1. AeroPQDs are fabricated by the adsorption of PQDs in the S-AIM, acting as a water barrier, and subsequently pumped by a blue LED chip to form a WLED.

moisture stability (stable over a few months in water). However, these organic-based polymer matrices generally exhibit low thermal conductivities and thermal stabilities, limiting the heat dissipation of organic polymer matrix-embedded PQDs in WLEDs.[40–42] In addition, most of the polymer matrices exhibit low stabilities under UV light.[43] These limitations set boundaries to the use of organic polymer matrix-embedded PQDs for integration in LED chips.[44,45] Furthermore, the combination of PQDs with other functional materials, such as Ag nanoparticles for plasmon-hot electron conversion[46] or Fe_3O_4 nanoparticles for magnetic control,[47] gradually becomes an essential topic to extend their range of applications. As the reported PQDs with high water stability are dispersed in an enclosed organic polymer matrix, their subsequent integration with functional materials is challenging because of the complicated embedding process and difficult post-treatment. Fortunately, PQDs can be easily integrated within mesoporous silica by a simple wet-mixing process.[48] This is one of the most promising methods to fabricate QD phosphor powders without complicated and time-consumed process of chemical reaction, which shows great potential in commercialization for white LED packaging. In addition, such protected PQDs with open structures also have a potential for working in tandem with other functional materials.

In order to explore the integration of highly water stable PQDs in open matrices, we therefore introduce superhydrophobic aerogel inorganic matrices (abbreviated "S-AIMs" in the following) with open structures as a water protection matrix and an integration platform for lead halide PQDs. These matrices can be simply combined with PQDs through a facile postadsorption process, preserving their PL properties and resulting in an excellent water stability. Then, the high optical and water/moisture-stable performances of PQDs integrated with the S-AIM (AeroPQDs) are verified by applying them to WLEDs. Finally, we show that other functional nanomaterials, such as the Fe_3O_4 nanoparticles can be integrated into our AeroPQDs due to the open structure. They have great potential as a fundamental fluorescence integration platform with high stability for compounding functional materials, expanding the application scope of PQDs.

2. Results and Discussion

AeroPQDs were obtained by a facile postadsorption process as illustrated in **Figure 1**. Photographs of the corresponding PQD solution, of the S-AIM powder, and of the resulting AeroPQD powders are shown in **Figure 2**a–c. Prepared by the anion exchange method,[49] AeroPQDs with various emission wavelength from blue to red (Figure 2d) are achieved, and exhibit strong PL under UV illumination. Transmission electron microscopy (TEM) is used to investigate the morphology of the fabricated AeroPQDs. TEM images of pristine green PQDs and SEM of the S-AIMs are reported in **Figure 3**a and Figure S1 (Supporting Information), respectively. Figure 3a shows PQDs with the cuboid shape with orthorhombic phase. The high resolution TEM image (inset) shows the [1 1 0] lattice planes of PQDs with an interplanar spacing d of 0.58 nm. The X-ray powder diffraction (XRD) pattern in Figure S2 (Supporting Information) shows peaks corresponding to the [0 0 1], [1 1 0], and [−2 0 0] crystal faces. These results confirm the successful synthesis of PQDs by the ultrasonic method.[50] Figure S1 (Supporting Information) shows S-AIMs with irregular shapes and randomly distributed particle size at 0.5–50 μm, which are

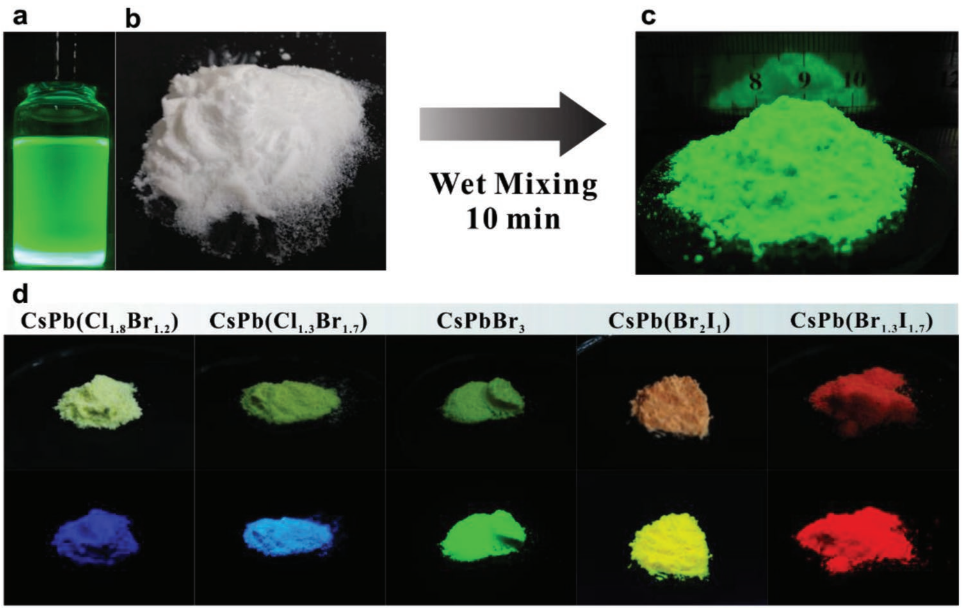

Figure 2. Photographs of a) $CsPbBr_3$/hexane PQD solution, b) S-AIM powders, and c) green AeroPQD powders obtained by wet-mixing of (a) and (b). Photographs of d) AeroPQD powders with different colors: blue, cyan, green, yellow, and red color (from left to right), respectively under sunlight illumination (top row) and UV light illumination (bottom row), and the composition of the product: $CsPb(Cl_{1.8}Br_{1.2})$, $CsPb(Cl_{1.3}Br_{1.7})$, $CsPbBr_3$, $CsPb(Br_2I_1)$, $CsPb(Br_{1.3}I_{1.7})$ (from left to right).

further confirmed by the scanning electron microscopy (SEM) images in Figure 3b. Such a rough surface originates from the randomly distributed pore structures, similar to a maze. These random pore structures and the rough surface lead to a combined effect, preventing the ambient moisture from penetrating into the S-AIMs, and as will be discussed in the following, serve for protecting the PQDs. Although S-AIMs have random pore structures, PQDs are found to be uniformly distributed in the S-AIMs, as observed from the TEM image of green AeroPQDs shown in Figure 3c,d. In addition, there are hardly any PQDs observed in the outer region of the S-AIMs (Figure 3c and Figure S3, Supporting Information), indicating the excellent adsorption of PQDs into S-AIMs. Most importantly, whereas PQDs are observed to be significantly aggregated in solution, as shown in Figure 3a; they show excellent dispersity upon integration into S-AIMs. Notably, because of aggregation-induced quenching, aggregation is found to be a serious issue that reduces the conversion efficiency when PQDs are directly used as phosphor powders or transferred into a polymer matrix for practical applications.[23,27,51] S-AIMs can effectively solve this issue since the PQD mean size of 22 nm (Figure S4, Supporting Information) is comparable to the S-AIM mean pore size of 20 nm (Figure S5, Supporting Information). The compatible pore size is the main reason why PQDs can be easily trapped inside S-AIMs through the postadsorption process.[48] The composition of PQDs and S-AIMs is further confirmed by the elemental maps of AeroPQDs, as shown in Figure 3e–h. Almost all the Cs and Pb of PQDs cover the Si regions of the S-AIMs, clearly demonstrating that AeroPQDs are formed by a facile postadsorption process. Additionally, the strong adsorption of PQDs within the S-AIMs was confirmed by mixing green and red AeroPQDs together in silicone and then by packaging them onto a blue LED to achieve white light, the green and red emission peaks are clearly observed without undergoing anion exchange, as shown in Figure S6 (Supporting Information). These results suggest that the AeroPQDs, which are highly compatible with the currently used WLED packaging processes, can effectively replace the common rare-earth-based phosphors.[13]

The optical performance of AeroPQDs was subsequently investigated and the results are presented in **Figure 4**. One should note that for the measurements, all the AeroPQD samples were used in solid form just like for phosphor particles. The emission spectra of AeroPQDs with blue, cyan, green, yellow, and red colors are given in Figure 4a–e, respectively. As observed, the AeroPQD samples exhibit spectra similar to those of PQD solutions without FWHM broadening (Table S1, Supporting Information), thus preserving excellent color purity for display applications. However, the peak wavelengths of AeroPQDs are slightly red shifted compared with those of the PQD solutions. Generally, aggregation and reabsorption can lead to a red shift.[52,53] Because the dispersion is excellent (Figure 3c,d), reabsorption and ligands loss are considered to be the possible factor causing the red shift of AeroPQD peak wavelengths. The subwavelength pore structures and large surface roughness of S-AIMs cause scattering of incident light (the corresponding transmittance and haze spectra are shown in Figure S7 in the Supporting Information), increasing its path length in the AeroPQDs.[25] As a result, the absorption of blue photons by the PQDs is enhanced, thus generating more down-converted light, but it also leads to a higher probability of the reabsorption events.[54,55] The PL intensity comparison plot (integrated from 480 to 580 nm) of the green AeroPQDs and green PQDs in solution confirms this explanation (Figure S8, Supporting Information). Please note that, although the PQD concentration is the same in these two samples, the PL intensity of green

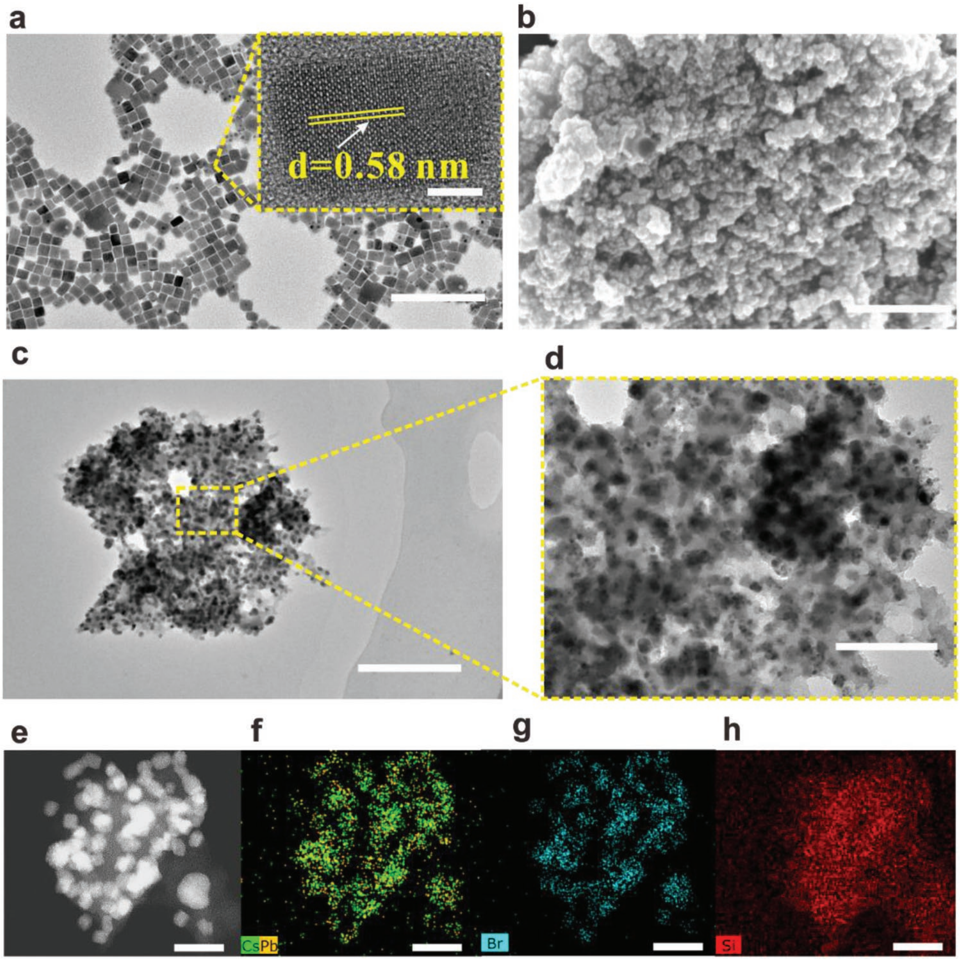

Figure 3. Morphology of the PQDs, S-AIMs, and AeroPQDs. a) TEM image of pristine green PQDs. The insert shows the lattice of single PQD, and the scale bars was 5 nm. b) SEM image of S-AIM. c) TEM image of green AeroPQDs. d) SEM image of green AeroPQDs and e–h) corresponding elemental maps. Scale bars of (a), (b), (c), (d), and (e)–(h) correspond to 200, 500, 500, 200, and 100 nm, respectively.

AeroPQDs is 1.23 times higher than that of green PQDs in solution, indicating enhanced green light emission from AeroPQDs at the same excitation. Therefore, although internal light scattering in S-AIMs causes a slight red shift, it is beneficial for enhancing the PL intensity of the integrated PQD. In addition, larger red shifts are observed for AeroPQDs at shorter emission wavelengths. The absorption spectra of the PQD solutions are given in Figure 4f. It is because that the absorption is stronger near the absorption edge for PQDs with shorter emission wavelength. PQDs with shorter emission wavelength can more easily lead to reabsorption (red shift in emission spectra) by enhancing the emission of short-wavelength light.

The PL decay curves of green AeroPQDs, blue AeroPQDs, and red AeroPQDs are given in Figure 4g and Figure S9a,b (Supporting Information), respectively, and they are compared with those of corresponding PQD solutions and PQD powders (obtained after drying the PQD solutions). Please note that the PL of blue and red PQD powders was too weak to be measured because of aggregation quenching and fast degradation;[27,48] therefore, it is not included here. The PL decay curves of the AeroPQDs were fitted using double exponential function or monoexponential function;[56] the fitted fast decay time t_1, slow decay time t_2, and the respective amplitudes a_1 and a_2 are listed in **Table 1**. Compared with the green PQD solution, the green PQD powder shows a slower PL decay, whereby t_2 increases from 9.9 to 25.7 ns. For PQDs, the electron transitions associated with surface states lead to a longer PL decay time,[57] indicating that the PQD powders obtained by drying the solutions possess more surface traps. For instance, the green PQD powder exhibits a PLQY of only 6.4%, which is significantly lower than that of the green PQD solution (PLQY of 83.2%). This is also the main reason why PQDs are difficult to be directly used as phosphor powders, limiting their application in commercial WLEDs. Moreover, the green AeroPQDs exhibit a longer PL decay time compared with the green PQD solution—t_{avg} increases from 8.4 to 10.5 ns; however, this value is still 59.6% lower than that of the green PQD powder (20.8 ns). These results indicate that the surface traps of green PQDs can be successfully suppressed by compositing with S-AIMs; though they are also achieved by evaporating the solution as in the preparation of the green PQD powder. This can be attributed to the good compatibility of S-AIMs with the oil solvent,

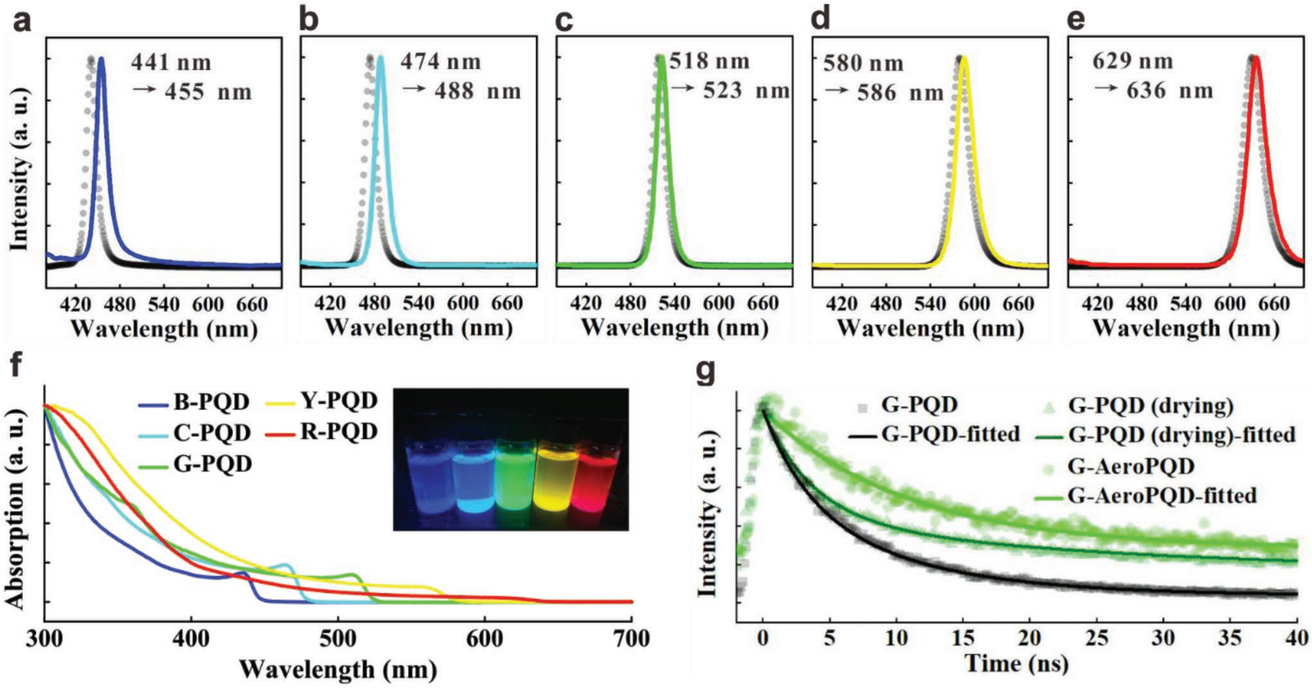

Figure 4. Normalized emission spectra of a) blue (B), b) cyan (C), c) green (G), d) yellow (Y), and e) red (R) AeroPQDs; the background dashed–dotted curves are the emission spectra of the corresponding pristine PQD solutions. f) Absorption spectra of PQD solutions with different emission wavelengths corresponding to (a)–(e), and the composition of the product was $CsPb(Cl_{1.8}Br_{1.2})$, $CsPb(Cl_{1.3}Br_{1.7})$, $CsPbBr_3$, $CsPb(Br_2I_1)$, $CsPb(Br_{1.3}I_{1.7})$, respectively. Time-dependent PL decay spectra of g) green AeroPQDs, green PQD solution, and green PQD powder (obtained after drying the PQD solution).

resulting from the presence of $-CH_3$ oleophylic functional groups on their surfaces. This explanation is indeed supported by the Fourier-transform IR (FTIR) spectra shown in Figure S10 (Supporting Information); which show absorption peaks at 2964 and 2905 cm^{-1} corresponding to the $-CH_3$ stretching vibration modes, and at 850 and 1257 cm^{-1} corresponding to the Si–C stretching and bending vibration modes, respectively. The S-AIMs can simultaneously adsorb ligands, including oleic acid and amines that bonded with PQDs during solution evaporation, suppressing the generation of surface defects by protecting the ligands against detachment from PQDs.[58–60] Therefore, the green AeroPQDs exhibit a high relative PLQY (the PLQY ratio of the pristine AeroPQDs to the pristine PQD solution) of 90.9% (absolute of 75.6%) compared to PQDs in solution. In addition, the PL decay time of green AeroPQDs is slightly longer than that of the green PQD solution, which is possibly caused by the trap states introduced by the S-AIMs. The PL decay curves of blue and red AeroPQDs are given in Figure 4h,i, respectively. Similarly, blue and red AeroPQDs exhibit longer PL decay times compared with the blue and red PQDs solutions, respectively. Moreover, hardly any PLQY reduction is observed for the blue and red PQDs after integration with S-AIMs. These results suggest that integration of PQDs with S-AIMs through the simple postadsorption process is a facile strategy to obtain well-dispersed PQD hybrid powders with excellent optical performances.

Table 1. PL decay fitting parameters: fast decay time t_1, slow decay time t_2, t_1 proportion a_1, t_2 proportion a_2, and average decay time t_{avg}, and PLQY of different PQD samples corresponding to Figure 4a–e; particularly, the PL decay curves of the AeroPQDs were fitted using monoexponential function.

Samples	t_1 [ns]	t_2 [ns]	a_1 [%]	a_2 [%]	t_{avg} [ns]	PLQY [%]
G-PQD solution	3.3	9.9	21.7	78.3	8.4	83.2
G-PQD powder	3.7	25.7	22.5	77.5	20.8	6.4
G-AeroPQD	–	–	–	–	10.5	75.6
B-PQD solution	1.6	14.2	55.0	45.0	7.3	5.5
B-AeroPQD	2.4	13.4	16.0	84.0	11.6	9.4
R-PQD solution	120.1	617.6	42.9	57.1	404.1	21.7
R-AeroPQD	–	–	–	–	–	10.1

Low reliability is one of the main factors limiting the practical applications of PQDs, especially their fast degradation in the presence of moisture.[20,22,24] Herein, we adopted the widely used green PQDs to investigate their reliability against moisture. Generally, PQDs are stored in the liquid state (dispersion) or solid state (without dispersion in solution). We compared the PL stability of green AeroPQDs and PQDs in their liquid states by adding water, as shown in **Figure 5**a. Please note that the green PQD concentration, solution volume, and volume of water added were the same for all samples, but different mass ratios of S-AIMs to green PQDs (AP:G-PQD) were used for the measurements. Although the green PQDs (AP:G-PQD = 0) are protected with the oily solution, their PL stability dramatically reduces with water addition after 72 h, and it reaches almost zero after 120 h. As the mass ratio increases, the PL stability improves with aging in water, particularly when the mass ratio

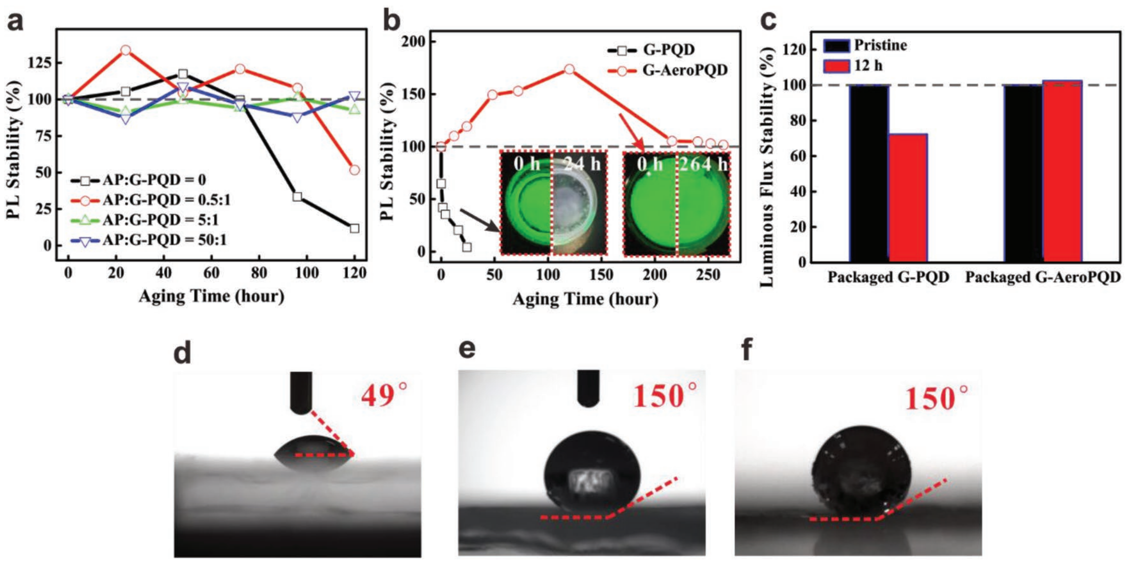

Figure 5. Improved water/moisture stability in AeroPQDs under aging tests. a) PL stability of green PQDs and AeroPQDs obtained after adding 3 mL water for different aging times (both were dispersed in 3 mL *n*-hexane with a PQD concentration of 10 mg mL^{-1}), and mass ratios of S-AIMs to green PQDs (AP:G-PQD) ranging from 0 to 50:1. b) PL stability of green PQDs and AeroPQDs entirely soaked in water for different aging times; the insert photographs are PQDs (left) and AeroPQD (right) powders soaked in water. c) Luminous flux stability of LEDs packaged with green PQDs and AeroPQDs and after moisture aging (temperature of 25 °C and humidity of 75%) for 12 h. Photographs of a water drop on d) bare glass, e) S-AIMs/glass, and f) green AeroPQDs/glass (S-AIMs and green AeroPQDs were coated on glass by spinning).

is 5:1, no reduction in PL stability occurs even after 120 h. Therefore, the moisture reliability of AeroPQDs with a suitable mass ratio is significantly stronger than that of PQDs when compared in the liquid state. Accordingly, the mass ratio of 5:1 was selected for all subsequent tests.

It is advisable to store PQDs in the solid state because their solutions are generally toxic and unstable.[61] Therefore, to confirm the moisture reliability of AeroPQDs, they were soaked in water without the protective solution, as shown in Figure S11a (Supporting Information). The PL stability plots of green PQDs and AeroPQDs (mass ratio of 5:1) entirely soaked in water for different times are given in Figure 5b. Without the protective solution, the PL stability of the green PQDs drastically decreases after being soaked in water. These PQDs undergo complete degradation after being soaked for 24 h and exhibit no PL under UV light illumination, as shown in the inset; the significantly blue-shifted spectra shown in Figure S12a,b (Supporting Information) confirm the degradation. On the other hand, AeroPQDs exhibit a high PL stability of 100% after being soaked in water for 264 h (11 days), as shown in Figure 5b, and a bright green color under UV light illumination, as shown in the inset. The spectra recorded after soaking AeroPQDs in water for different times are given in Figure S12c,d (Supporting Information); interestingly, a slight red shift rather than blue shift (exhibited by PQDs) is observed and the PL intensity for G-AeroPQD increased a lot at the beginning stage (0–120 h) as shown in Figure 5b. One reasonable explanation is that a part of the surface defective layer of $CsPbBr_3$ PQDs dissolves in water, leading to enhancement in the PL of PQDs;[62] thus, PQDs emit much more green light after being soaked in water. In addition, the PL intensity for G-AeroPQD keeps at 100% after 180 h soaked in water, which means that the $CsPbBr_3$ on the surface of S-AIMs have almost dissolved in water while $CsPbBr_3$ trapped into the pore were protected. Moreover, the photographs of AeroPQDs soaked in water for 3.5 months are given in Figure S11b (Supporting Information) further proved it. The volume of AeroPQDs significantly increases because of the adsorption of water in between S-AIMs; however, they exhibit a bright green color under UV illumination and high PLQY stability of 50.5%. The reliability of our AeroPQDs with open structure is comparable to that of previously reported PQDs embedded in an enclosed organic polymer matrix,[33–35] and higher than that of PQDs embedded in all inorganic matrices.[16–20,26] Please note that in some previous studies, the reliability of PQDs was evaluated by placing them on water instead of soaking them. For comparison, we also conducted an aging test after placing the AeroPQDs on water and sealing them in a bottle, as shown in Figure S11c (Supporting Information), these AeroPQDs maintain a high PLQY stability of 77.6% after 4.5 months, and to the best of our knowledge, such a high water reliability for the PQD powder integrating with the open matrix has not yet been reported.

Moreover, the moisture reliability of AeroPQDs packaged in LEDs was determined under aging tests (temperature of 25 °C and humidity of 75%); the results obtained for green PQDs and AeroPQDs are given in Figure 5c (the packaging structure and PQD concentration are the same in both cases). The luminous flux of LEDs packaged with green PQDs significantly drops below 70% after 12 h, and therefore, it does not satisfy the LM70 lifetime requirement, according to the Energy Star standard.[63] In contrast, LEDs packaged with AeroPQDs do not exhibit a reduction in luminous flux under the same aging conditions. The respective electroluminescence (EL) spectra are given in Figure S13 (Supporting Information), and highlight the superior water stability of LEDs packaged with green AeroPQDs. In addition, the latter exhibit a higher intensity of green peak compared to that packaged with green PQDs, further confirming the PL enhancement effect of S-AIMs integrated with PQDs, as discussed above. The good stability may arise from the superhydrophobic properties of AeroPQDs, which is confirmed by contact angle measurements with water. The contact angle of bare glass is only 49°, as shown in Figure 5d. Both S-AIMs and AeroPQDs coated on glass indeed exhibit the same contact angle of 150°, as shown in Figure 5e,f, respectively. Detailed information about the superhydrophobic property of AeroPQDs can be obtained from Video S1 (Supporting Information).

The mechanisms of AeroPQDs against water are further investigated by introducing two kinds of open matrices, a less hydrophobic aerogel and the SBA-15 mesoporous silica (contact angles shown in Figure S14 in the Supporting Information), respectively. The less hydrophobic aerogel features a similar pore structure as the S-AIM, yet their surface −OH groups have not been replaced by the $-CH_3$ groups. The SBA-15 mesoporous silica is with a regular hexagonal pore structure and a pore size of 11 nm.[64] Both of these open matrices are integrated with PQDs according to the same adsorption process, and a water test is carried out for these protected PQD powders as shown in Figure S15 (Supporting Information). In Figure S15a (Supporting Information), the protected PQDs integrated with SBA-15 show almost no PL after only 10 min, which is similar to that of PQD powders without protection. One reasonable explanation is that PQDs can be only adsorbed on the surface of SBA-15 due to the mismatched size between the pore and the particle, which is verified by the TEM image shown in Figure S16 (Supporting Information). Therefore, the matched size is necessary for a high water stability by sufficiently adsorbing PQDs inside the open matrix. Furthermore, the protected PQDs integrated with the less hydrophobic aerogel achieves strong PL even after 24 h as shown in Figure S15b (Supporting Information), and are hence more stable than the PQD powders without protection (see Figure 5b) and then the protected PQDs integrated with SBA-15 (see Figure S15a in the Supporting Information). These results clearly indicate that the aerogel is beneficial to enhance the water stability of PQDs mainly owing to the hydrophobicity induced by the rough surface.[65] In addition, the internal porous structure also helps obstructing water by increasing its path before getting into contact with the adsorbed PQDs, which is the main reason why AeroPQDs soaked in water expand while still maintaining a high PLQY. Most importantly, the less hydrophobic aerogel leads to a faster degradation of PQDs in water compared with the S-AIMs. Almost no PL can be observed after only 5 days (120 h) using the less hydrophobic aerogel; whereas the AeroPQDs do not degrade in water even after 11 days (264 h). Therefore, only the pore structure is not enough to provide an excellent water stability for PQDs, the oleophylic functional groups on the pore structure are also necessary by further preventing the water to penetrate into the inner pores. Previous studies on the enclosed polymer organic matrix indicate that the surface structure plays the key role to enhance the water stability for PQDs,[34] however, it shows great differences in the situation for protected PQDs with open structure. The matched size between the pore and the particle, the hydrophobic rough surface, and the oleophylic functional groups are three factors to achieve an excellent water stability for PQDs in the open matrix. In addition, the photoexposure reliability of green AeroPQDs was also investigated, as shown in Figure S17 (Supporting Information). The AeroPQDs maintain a PL intensity of 50% after aging for 49 h (24 h under UV irradiance with 6 W output optical power); on the other hand, the PL intensity of PQDs dramatically drops to below 20% after UV irradiance for 6 h.[12]

After demonstrating the remarkable stability of the AeroPQDs against water and UV irradiance, their performance in WLEDs was then thoroughly analyzed. The green AeroPQDs, commercial red KSF phosphor, and a blue LED chip were adopted to achieve white light. The injection current-dependent luminous flux/efficacy and EL spectra of AeroPQD WLEDs are given in **Figure 6**a,b, respectively; a high luminous efficacy of 59.8 lm W^{-1} is achieved at a typical injection current of 20 mA and correlated color temperature (CCT) of ≈6500 K. To confirm the environmental stability of the AeroPQD WLED, a conventional PQD WLED was fabricated by replacing the green AeroPQDs with the green PQDs. It should be noted that the phosphor concentration is controlled to make the PQD WLED exhibit an emission spectrum similar to that of the AeroPQD WLED, ensuring a fair comparison. The EL spectra of the pristine WLED and of the aged WLED (under temperature of 25 °C and humidity of 75% for 7 days) are given in Figure 6c. As observed, the AeroPQD and PQD WLEDs exhibit similar initial spectra, and the AeroPQD LED shows negligible changes in emission after being exposed to air. However, the PQD WLED exhibits a significant intensity reduction (>50%) of its green peak, indicating that AeroPQDs provide better environmental stability to WLEDs because of their excellent performance, as aforementioned. Moreover, the luminous efficacies of AeroPQD and PQD WLEDs are compared in Figure 6d; the pristine AeroPQD WLED exhibits a luminous efficacy of 59.8 lm W^{-1}, which is 11.8% higher than that of pristine PQD WLED. Notably, it is barely reported that the protection shell of PQDs can enhance the optical performance for WLEDs. One reasonable explanation is that the integration with S-AIMs causes enhancement in the PL of PQDs; thus, the AeroPQD WLED with a lower PQD concentration of 0.5 wt% exhibits a green photon energy similar to that of the PQD WLED with a higher PQD concentration of 1.0 wt%. Generally, a low QD concentration is beneficial for achieving reduced reabsorption losses, leading to higher efficiencies.[14] After moisture aging for 7 days, the luminous efficacy of AeroPQD WLED slightly increases to106%; on the other hand, the luminous efficacy of the PQD WLED significantly drops to 74%. Moreover, the changes in the color coordinates determined for the PQD and AeroPQD WLEDs are given in Figure 6e. As observed, the AeroPQD WLED exhibits negligible change in the color coordinates and CCT of ≈6500 K, and emits a pure white color even after 7 days (left inset in Figure 6e). Conversely, the color coordinates of the PQD WLED significantly shift from (0.31, 0.33) to (0.37, 0.27), and its CCT decreases from ≈6500 to 3200 K, resulting in a reddish white color (right inset in Figure 6e). Thus, our results show that highly efficient and stable WLEDs can be achieved by using AeroPQDs, which accelerating their practical applications.

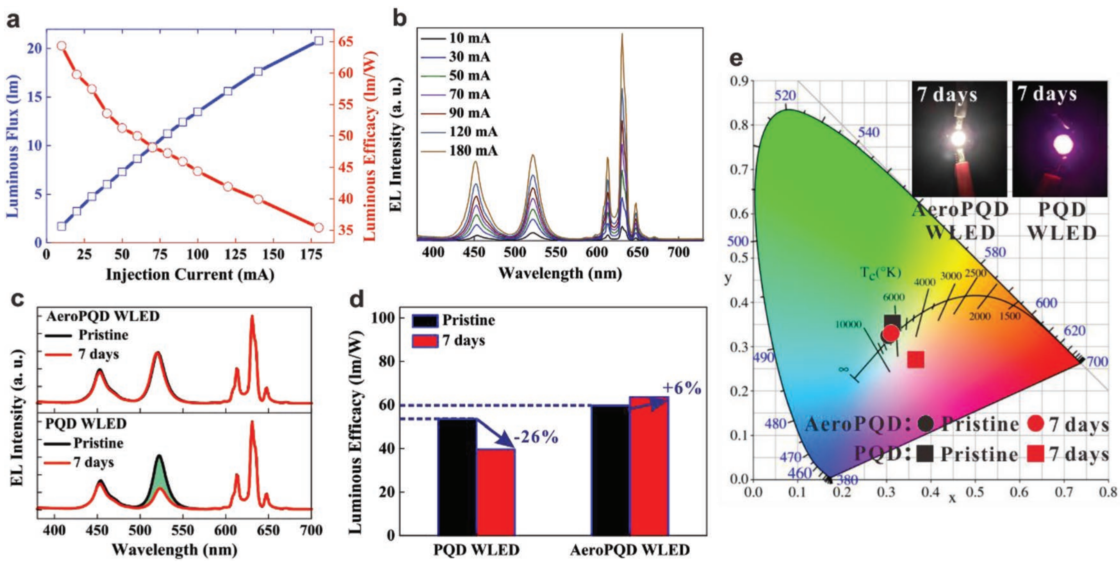

Figure 6. a) Injection current-dependent luminous flux/efficacy and b) EL spectra of AeroPQD WLEDs. c) EL spectra, d) luminous efficacy, and e) CIE 1931 color coordinates of AeroPQD and PQD WLEDs before and after moisture aging for 7 days (temperature of 25 °C, humidity of 75%); the measured current is 20 mA.

Since the S-AIM is an open integration platform, our AeroPQDs can be easily integrated with other nanoparticles to add new functionalities. Herein, we have adopted Fe_3O_4 nanoparticles as an example, and the obtained Fe_3O_4-AeroPQD powders with different mass ratio of S-AIM to Fe_3O_4 are shown in Figure S19 (Supporting Information). The XRD pattern of Fe_3O_4-AeroPQDs in **Figure 7**a confirms the presence Fe_3O_4 nanoparticles, which a corresponding peak at 35.5° (other peaks belong to AeroPQDs as shown in Figure S2 in the Supporting Information). The PL spectrum of Fe_3O_4-AeroPQDs with different mass ratio is given in Figure 7b. It is evident that the increased content of Fe_3O_4 nanoparticles can reduce the PL intensity due to their strong absorption on visible light; however, there is no influence on the critical performances for display applications including the peak location and the FWHM as shown in the insert, moreover black nanoparticles may help to improve the contrast of the display. It should be noticed that the PL from PQDs will entirely disappear when the mass ratio reaches 3:1, therefore, a suitable mass ratio larger than 9:1 is selected for subsequent characterizations. The hysteresis curve of Fe_3O_4-AeroPQDs is given in Figure 7c. It is confirmed that these hybrid particles have preserved the magnetic properties originated from Fe_3O_4 nanoparticles. As summarized in the left insert figure, a small mass ratio is beneficial to achieve a high

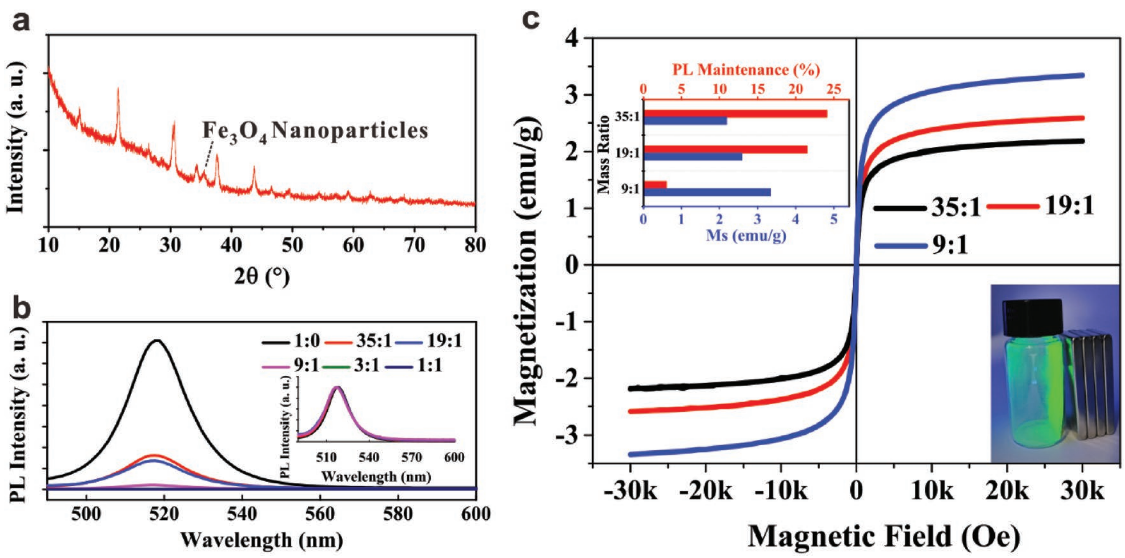

Figure 7. a) XRD pattern, b) PL spectra, and c) hysteresis curve of the Fe_3O_4-AeroPQD. The left insert figure in (c) is the PL stability corresponding to AeroPQDs and the saturation magnetization (M_s) of Fe_3O_4-AeroPQD with different mass ratio; the right insert image is Fe_3O_4-AeroPQDs with a mass ratio of 19:1 moved to the lateral of the bottle by the magnetic field.

saturation magnetization (M_s) as high as 3.34 emu g^{-1}, simultaneously resulted in a lower PL stability (corresponding to AeroPQDs). Typically, the Fe_3O_4-AeroPQDs can achieve a PL stability of 21.5% and a M_s of 2.59 emu g^{-1} at a mass ratio of 19:1. Therefore, the magnetization performance is enough to expand PQDs in new applications related to the magnetic manipulation as shown in the inset image and the Video S2 (Supporting Information).

3. Conclusion

In this work, we have proposed superhydrophobic AeroPQDs obtained by integrating presynthesized PQDs with the open platform of S-AIMs via a facile and cost-effective postadsorption process. Compared to PQDs in the liquid-state, AeroPQDs in the solid-state exhibit excellent optical performances, particularly the green AeroPQDs exhibit a high relative PLQY of 90.9%. The high performances are attributed to the presence of S-AIMs with oleophylic functional groups and suitable pore size, which serve as good dispersion matrices for PQDs during solution evaporation, suppressing particle aggregation and surface defects. Most importantly, AeroPQDs exhibit excellent water/moisture stability. It has been found that the matched size between the pore and the particle, the surface oleophylic functional group, and the hydrophobic rough surface (randomly pore structures) are three important factors for PQDs against water even in the open matrix, which is different to previous proposed mechanisms of PQDs in the enclosed matrix. As a result, AeroPQDs show no decay in PL intensity after being entirely soaked in water for 11 days, and exhibit a PLQY stability of 50.5% even after 3.5 months; on the other hand, the conventional PQDs fail to exhibit PL after being soaked in water for a day. Because of the presence of the protective S-AIMs that suppress surface defects and block moisture, AeroPQDs also exhibit higher irradiance stability compared with PQDs. The AeroPQDs maintain a PL intensity of 50% after aging for 49 h (24 h under UV irradiance with 6 W output optical power); on the other hand, the PL intensity of PQDs dramatically drops to below 20% after UV irradiance for 6 h. Consequently, highly efficient and stable WLEDs could be realized by using green AeroPQDs and red KSF phosphor. Notably, the AeroPQD WLED exhibits 11.8% higher initial luminous efficacy (59.8 lm W^{-1}) than the PQD WLED with the same output color. These results are attributed to the PL enhancement caused by the scattering effect of S-AIMs. Importantly, the conventional PQD WLED shows a luminous efficacy stability of 74%, as well as a large shift in color coordinates and CCT change from ≈6500 to 3200 K after a moisture aging (temperature of 25 °C and humidity of 75%) for 7 days. Conversely, our AeroPQD WLED exhibits a negligible change in luminous efficacy and color coordinates after aging for the same time because of the excellent stability of AeroPQDs. In addition, it is confirmed that our AeroPQDs can be easily integrated with functional nanoparticles due to the open structure, as demonstrated with magnetic Fe_3O_4 nanoparticles. Therefore, in addition to the application in conventional WLEDs, the proposed AeroPQDs can be a fundamental fluorescence integration platform with high stability for compounding different functional materials, expanding the application scope of PQDs.

4. Experimental Section

Materials: Cesium carbonate (Cs_2CO_3, 99%), lead (II) halide (PbX2, 99%), 1-octadecene (ODE, 90%), oleic acid (OA, 90%), and oleylamine (OAm, 90%) were purchased from Alfa Aesar. Hexane and silicone were purchased from Sigma-Aldrich and Dow Corning, respectively. S-AIMs and less hydrophobic aerogel were purchased from Suzhou Hengqiu Nano Reagent. SBA-15 was purchased by Nangjing XianFeng Nano. Fe_3O_4 (20 nm) was purchased by Shanghai Xangtian Nano Materials Co., Ltd. All chemicals were used as received without further purification.

Synthesis of All-Inorganic Colloidal $CsPbX_3$ PQDs: $CsPbBr_3$ was synthesized by an modified ultrasonic method, which based on our previous study.[46] Briefly, $PbBr_2$ (0.11 g), Cs_2CO_3 (0.0326 g), OA (0.1 mL), OAm (2 mL), and ODE (10 mL, liquid paraffin was replaced in our previous study) were mixed in a 30 mL bottle flask. Then, the reaction medium was subjected to tip-sonication (FS-300N, Ultrasonic Processor) at a power of 90 W (30% of the total power) for 1 h. During sonication, the colorless reaction solution gradually transformed into yellow, and then, orange-yellow. After the reaction, the reaction mixture was cooled to room temperature using an ice/water bath. The crude solution was centrifuged for 10 min at 10 000 rpm. Next, the obtained precipitate was dispersed in hexane (10 mL) and centrifuged for 5 min at 2500 rpm; large particles and agglomerated precursors were discarded in this step. The precipitate was then discarded, and the solution was preserved. The clear solution was placed in a refrigerator at 4 °C for further use. A series of all-inorganic colloidal $CsPbX_3$ (X = Cl, Br, I) PQDs were fabricated via the anion exchange reaction at room temperature. Typically, $PbCl_2$ or PbI_2 (0.1 mmol) was added into a 10 mL glass vial containing anhydrous hexane (5 mL), OA (0.5 mL), and OAm (0.5 mL) at 60 °C in a glove box. Next, the bottle was stirred for 2 h to fully dissolve the powders. For the anion exchange reaction, first, the obtained crude solution of $CsPbBr_3$ PQDs (2 mL) was added into a glass vial under vigorous stirring. Then, the prepared anion source (1.2 mL) was added in the diluted $CsPbBr_3$ PQD solution at room temperature.

Synthesis of AeroPQD Phosphor: In this procedure, $CsPbBr_3$/hexane solution (1 mL) was mixed with S-AIMs in a specific mass ratio. The resulting solution was sonicated for 1 min to properly disperse the S-AIMs. Then, the dispersion was dried at normal temperature with continuous stirring to obtain the AeroPQD phosphor. The cleaning process was further conducted by dispersing AeroPQD phosphor into hexane solution, and then centrifugated to acquire precipitation. This process was repeated 3 times until the supernatant is clear, which aim to remove $CsPbBr_3$ on the surface of aerogel.

Fabrication of WLEDs: Typically, the AeroPQD powder (0.05 g) and KSF powder (0.24 g) were mixed in silicone (3 mL) and stirred for 1 h using the magnetic stirrer. Then, the mixture was deactivated in vacuum to remove bubbles. Finally, the mixture was injected into a lead frame bonded with a blue LED chip to obtain the WLED.

Fabrication of Fe_3O_4-AeroPQDs: In this procedure, a certain amount of Fe3O4(1.4 mg,2.6 mg,5.6 mg) and S-AIMs (0.05 g) were dispersed into 5 mL *n*-hexane and then ultrasonic for 5 min. After volatilization and drying at normal temperature with continuous stirring, the Fe_3O_4-Aero was obtained. Then $CsPbBr_3$/hexane solution (1 mL) was added, the next steps are similar to "Synthesis of AeroPQD Phosphor" and Fe_3O_4-AeroPQDs was obtained.

Characterization: The crystal structures and surface morphologies of the prepared PQDs and S-AIMs were characterized by TEM (JEM-2100F, JEOL) with an accelerating voltage of 200 kV and field-emission SEM (Zeiss, Merlin). High-resolution TEM (HRTEM) and high-angle annular dark field scanning TEM (HAADF-STEM) images were obtained using a high-voltage TEM instrument (XFlash 5030T). The phase of the as-prepared PQDs were measured by X-ray diffraction (XRD, D8-Advance, Bruker) with a Cu Kα radiation source (λ = 0.15418 nm) at a counting rate of 10° min^{-1} in the scanning angle (2θ) range from 10° to 80°. FTIR spectroscopy was performed using an IR spectrometer (VERTEX 33, Bruker). The UV–vis absorption spectra of the PQDs were recorded using a UV–vis spectrometer (Shimadzu) in the wavelength range from 300 to 700 nm, at 1 nm intervals. The PL spectra of the PQDs were recorded using a fluorescence spectrophotometer (RF-6000, Shimadzu) using a Xe lamp as an excitation source (Before the PL measurement for AeroPQDs solution, the mixture was dispersed by ultrasonic treatment for 10 s due to sedimentation). The time-resolved fluorescence spectra were recorded on a steady-state fluorescence spectrometer (FLS1000, Edinburgh).The PLQYs of the samples were measured using an absolute PLQY spectrometer under an excitation wavelength of 365 nm (K.K. C9920, Hamamatsu Photonics). The N_2 adsorption/desorption isotherms and pore size distributions of the S-AIMs were obtained using a gas adsorption analyzer (TriStar II 3flex, Mike). The hysteresis curve was measured by Squid-VSM. All reliability tests were conducted under laboratory conditions at a constant ambient temperature of 25 °C.

Supporting Information

Supporting Information is available from the Wiley Online Library or from the author.

Acknowledgements

This work was supported by the National Natural Science Foundation of China (51775199, 51735004), Natural Science Foundation of Guangdong Province (2018B030306008), the Project of Science and Technology New Star in Zhujiang Guangzhou City (201806010102), the Karlsruhe School of Optics & Photonics (KSOP), and the China Scholarship Council (201706150050).

Conflict of Interest

The authors declare no conflict of interest.

Keywords

luminous efficacy, perovskite quantum dots, stability, superhydrophobic aerogel inorganic matrices, white light-emitting diodes

Received: October 19, 2019
Revised: December 4, 2019
Published online:

[1] J. Song, J. Li, X. Li, L. Xu, Y. Dong, H. Zeng, *Adv. Mater.* **2015**, *27*, 7162.
[2] Y. Tong, E. Bladt, M. F. Aygüler, A. Manzi, K. Z. Milowska, V. A. Hintermayr, P. Docampo, S. Bals, A. S. Urban, L. Polavarapu, *Angew. Chem., Int. Ed.* **2016**, *55*, 13887.
[3] L. Protesescu, S. Yakunin, M. I. Bodnarchuk, F. Krieg, R. Caputo, C. H. Hendon, R. X. Yang, A. Walsh, M. V. Kovalenko, *Nano Lett.* **2015**, *15*, 3692.
[4] M. V. Kovalenko, L. Protesescu, M. I. Bodnarchuk, *Science* **2017**, *358*, 745.
[5] H. Huang, A. S. Susha, S. V. Kershaw, T. F. Hung, A. L. Rogach, *Adv. Sci.* **2015**, *2*, 1500194.
[6] Y. Kim, E. Yassitepe, O. Voznyy, R. Comin, G. Walters, X. Gong, P. Kanjanaboos, A. F. Nogueira, E. H. Sargent, *ACS Appl. Mater. Interfaces* **2015**, *7*, 25007.
[7] J. Pan, S. P. Sarmah, B. Murali, I. Dursun, W. Peng, M. R. Parida, J. Liu, L. Sinatra, N. Alyami, C. Zhao, *J. Phys. Chem. Lett.* **2015**, *6*, 5027.
[8] P. Pust, P. J. Schmidt, W. Schnick, *Nat. Mater.* **2015**, *14*, 454.
[9] M. Liu, G. Zhong, Y. Yin, J. Miao, K. Li, C. Wang, X. Xu, C. Shen, H. Meng, *Adv. Sci.* **2017**, *4*, 1700335.
[10] M. Cao, Y. Xu, P. Li, Q. Zhong, D. Yang, Q. Zhang, *J. Mater. Chem. C* **2019**, *7*, 14412.
[11] S. Huang, Z. Li, B. Wang, N. Zhu, C. Zhang, L. Kong, Q. Zhang, A. Shan, L. Li, *ACS Appl. Mater. Interfaces* **2017**, *9*, 7249.
[12] H. Moon, C. Lee, W. Lee, J. Kim, H. Chae, *Adv. Mater.* **2019**, *31*, 1804294.
[13] S. Ye, F. Xiao, Y. Pan, Y. Ma, Q. Zhang, *Mater. Sci. Eng., R* **2010**, *71*, 1.
[14] J. S. Li, Y. Tang, Z. T. Li, X. R. Ding, L. S. Rao, B. H. Yu, *IEEE Trans. Electron Devices* **2018**, *65*, 2877.
[15] X. Tang, J. Yang, S. Li, Z. Liu, Z. Hu, J. Hao, J. Du, Y. Leng, H. Qin, X. Lin, *Adv. Sci.* **2019**, *6*, 1900412.
[16] S. Ye, J.-Y. Sun, Y.-H. Han, Y.-Y. Zhou, Q.-Y. Zhang, *ACS Appl. Mater. Interfaces* **2018**, *10*, 24656.
[17] J. Y. Sun, F. T. Rabouw, X. F. Yang, X. Y. Huang, X. P. Jing, S. Ye, Q. Y. Zhang, *Adv. Funct. Mater.* **2017**, *27*, 1704371.
[18] Y. Cheng, C. Shen, L. Shen, W. Xiang, X. Liang, *ACS Appl. Mater. Interfaces* **2018**, *10*, 21434.
[19] S. Yuan, D. Chen, X. Li, J. Zhong, X. Xu, *ACS Appl. Mater. Interfaces* **2018**, *10*, 18918.
[20] Y. Wei, H. Xiao, Z. Xie, S. Liang, S. Liang, X. Cai, S. Huang, A. A. Al Kheraif, H. S. Jang, Z. Cheng, *Adv. Opt. Mater.* **2018**, *6*, 1701343.
[21] S. Guarnera, A. Abate, W. Zhang, J. M. Foster, G. Richardson, A. Petrozza, H. J. Snaith, *J. Phys. Chem. Lett.* **2015**, *6*, 432.
[22] A. Loiudice, S. Saris, E. Oveisi, D. T. Alexander, R. Buonsanti, *Angew. Chem., Int. Ed.* **2017**, *56*, 10696.
[23] Z. Li, L. Kong, S. Huang, L. Li, *Angew. Chem.* **2017**, *129*, 8246.
[24] C. Sun, Y. Zhang, C. Ruan, C. Yin, X. Wang, Y. Wang, W. W. Yu, *Adv. Mater.* **2016**, *28*, 10088.
[25] X. Li, Y. Wang, H. Sun, H. Zeng, *Adv. Mater.* **2017**, *29*, 1701185.
[26] Z. Liu, Y. Zhang, Y. Fan, Z. Chen, Z. Tang, J. Zhao, Y. Lv, J. Lin, X. Guo, J. Zhang, *ACS Appl. Mater. Interfaces* **2018**, *10*, 13053.
[27] V. Malgras, J. Henzie, T. Takei, Y. Yamauchi, *Angew. Chem.* **2018**, *130*, 9019.
[28] Z. Hu, Z. Liu, Y. Bian, S. Li, X. Tang, J. Du, Z. Zang, M. Zhou, W. Hu, Y. Tian, *Adv. Opt. Mater.* **2018**, *6*, 1700997.
[29] Q. Zhong, M. Cao, H. Hu, D. Yang, M. Chen, P. Li, L. Wu, Q. Zhang, *ACS Nano* **2018**,*12*, 8579.
[30] Z. J. Li, E. Hofman, J. Li, A. H. Davis, C. H. Tung, L. Z. Wu, W. Zheng, *Adv. Funct. Mater.* **2018**, *28*, 1704288.
[31] Y. Wei, X. Deng, Z. Xie, X. Cai, S. Liang, P. A. Ma, Z. Hou, Z. Cheng, J. Lin, *Adv. Funct. Mater.* **2017**, *27*, 1703535.
[32] X. Shen, C. Sun, X. Bai, X. Zhang, Y. Wang, Y. Wang, H. Song, W. W. Yu, *ACS Appl. Mater. Interfaces* **2018**, *10*, 16768.
[33] Y. Xin, H. Zhao, J. Zhang, *ACS Appl. Mater. Interfaces* **2018**, *10*, 4971.
[34] T. Xuan, J. Huang, H. Liu, S. Lou, L. Cao, W. Gan, R.-S. Liu, J. Wang, *Chem. Mater.* **2019**, *31*, 1042.
[35] Q. Zhou, Z. Bai, W. g. Lu, Y. Wang, B. Zou, H. Zhong, *Adv. Mater.* **2016**, *28*, 9163.
[36] A. Pan, M. J. Jurow, F. Qiu, J. Yang, B. Ren, J. J. Urban, L. He, Y. Liu, *Nano Lett.* **2017**, *17*, 6759.
[37] Y. Wang, J. He, H. Chen, J. Chen, R. Zhu, P. Ma, A. Towers, Y. Lin, A. J. Gesquiere, S. T. Wu, *Adv. Mater.* **2016**, *28*, 10710.
[38] A. Pan, J. Wang, M. J. Jurow, M. Jia, Y. Liu, Y. Wu, Y. Zhang, L. He, Y. Liu, *Chem. Mater.* **2018**, *30*, 2771.

[39] H. Liao, S. Guo, S. Cao, L. Wang, F. Gao, Z. Yang, J. Zheng, W. Yang, *Adv. Opt. Mater.* **2018**, *6*, 1800346.
[40] B. Xie, H. Liu, R. Hu, C. Wang, J. Hao, K. Wang, X. Luo, *Adv. Funct. Mater.* **2018**, *28*, 1801407.
[41] J. Y. Woo, K. N. Kim, S. Jeong, C.-S. Han, *Nanotechnology.* **2010**, *21*, 495704.
[42] S. D. Yu, Y. Tang, Z. T. Li, K. H. Chen, X. R. Ding, B. H. Yu, *Photonics Res.* **2018**, *6*, 90.
[43] J.-Y. Bae, Y. Kim, H. Kim, Y. Kim, J. Jin, B.-S. Bae, *ACS Appl. Mater. Interfaces* **2015**, *7*, 1035.
[44] C. Sun, Y. Zhang, S. Kalytchuk, Y. Wang, X. Zhang, W. Gao, J. Zhao, R. Zboril, K. Safarova, W. W. Yu, *J. Mater. Chem. C* **2015**, *3*, 6613.
[45] Y. Wang, S. Kalytchuk, Y. Zhang, H. Shi, S. V. Kershaw, A. L. Rogach, *J. Phys. Chem. Lett.* **2014**, *5*, 1412.
[46] X. Huang, H. Li, C. Zhang, S. Tan, Z. Chen, L. Chen, Z. Lu, X. Wang, M. Xiao, *Nat. Commun.* **2019**, *10*, 1163.
[47] S. Jiang, Y. Hu, H. Wu, Y. Zhang, Y. Zhang, Y. Wang, Y. Zhang, W. Zhu, J. Li, D. Wu, J. Chu, *Adv. Mater.* **2019**, *31*, 1807507.
[48] H. C. Wang, S. Y. Lin, A. C. Tang, B. P. Singh, H. C. Tong, C. Y. Chen, Y. C. Lee, T. L. Tsai, R. S. Liu, *Angew. Chem.* **2016**, *128*, 8056.
[49] G. Nedelcu, L. Protesescu, S. Yakunin, M. I. Bodnarchuk, M. J. Grotevent, M. V. Kovalenko, *Nano Lett.* **2015**, *15*, 5635.
[50] L. Rao, Y. Tang, C. Song, K. Xu, E. T. Vickers, S. Bonabi Naghadeh, X. Ding, Z. Li, J. Z. Zhang, *Chem. Mater.* **2019**, *31*, 365.
[51] X. Li, Y. Liu, X. Song, H. Wang, H. Gu, H. Zeng, *Angew. Chem., Int. Ed.* **2015**, *54*, 1759.
[52] J. Li, Y. Tang, Z. Li, K. Cao, C. Yan, X. Ding, *Nanotechnology* **2018**, *29*, 295707.
[53] W. Zhang, D. Dai, X. Chen, X. Guo, J. Fan, *Appl. Phys. Lett.* **2014**, *104*, 6726.
[54] C. Sommer, F. Reil, J. R. Krenn, P. Hartmann, P. Pachler, H. Hoschopf, F. P. Wenzl, *J. Lightwave Technol.* **2011**, *29*, 2285.
[55] J. Lee, K. Min, Y. Park, K. S. Cho, H. Jeon, *Adv. Mater.* **2018**, *30*, 1703506.
[56] J. Yang, X. Wen, H. Xia, R. Sheng, Q. Ma, J. Kim, P. Tapping, T. Harada, T. W. Kee, F. Huang, *Nat. Commun.* **2017**, *8*, 14120.
[57] V. S. Chirvony, S. González-Carrero, I. Suárez, R. E. Galian, M. Sessolo, H. J. Bolink, J. P. Martínez-Pastor, J. Pérez-Prieto, *J. Phys. Chem. C* **2017**, *121*, 13381.
[58] S. Sadeghi, B. G. Kumar, R. Melikov, M. M. Aria, H. B. Jalali, S. Nizamoglu, *Optica* **2018**, *5*, 793.
[59] J.-S. Li, Y. Tang, Z.-T. Li, L.-S. Rao, X.-R. Ding, B.-H. Yu, *Photonics Res.* **2018**, *6*, 1107.
[60] T. L. Shen, K. J. Chen, C. W. Sher, H. V. Han, K. Y. Wang, J. R. Li, C. C. Lin, M. H. Shih, C. C. Fu, H. C. Kuo, *Nanoscale* **2016**, *8*, 1117.
[61] J. Li, Y. Tang, Z. Li, X. Ding, L. Rao, B. Yu, *Opt. Lett.* **2019**, *44*, 90.
[62] Y. Liu, F. Li, Q. Liu, Z. G. Xia, *Chem. Mater.* **2018**, *30*, 6922.
[63] L. Trevisanello, M. Meneghini, G. Mura, M. Vanzi, M. Pavesi, G. Meneghesso, E. Zanoni, *IEEE Trans. Device Mater. Reliab.* **2008**, *8*, 304.
[64] J. Li, Y. Tang, Z. Li, X. Ding, B. Yu, L. Lin, *ACS Appl. Mater. Interfaces* **2019**, *11*, 18808.
[65] M. Liu, S. Wang, L. Jiang, *Nat. Rev. Mater.* **2017**, *2*, 17036.